# Discovery of pyrazolones as novel carboxylesterase 2 inhibitors that potently inhibit the adipogenesis in cells

Xing-Kai Qian [a],[1], Jing Zhang [a],[1], Pei-Fang Song [a], Yi-Su Zhao [a], Hong-Ying Ma [a], Qiang Jin [a], Dan-Dan Wang [a], Xiao-Qing Guan [a], Shi-Yang Li [c], XiaoZe Bao [b],[*], Li-Wei Zou [a],[*]

[a] Institute of Interdisciplinary Integrative Medicine Research, Shanghai University of Traditional Chinese Medicine, Shanghai 201203, China
[b] College of Pharmaceutical Science & Collaborative Innovation Center of Yangtze River Delta Region Green Pharmaceuticals, Zhejiang University of Technology, Hangzhou 310014, China
[c] Analytical Central Laboratory, Shengyang Harmony Health Medical Laboratory Co Ltd, 19 Wen Hui Road Shenyang 210112, China

ABSTRACT

Carboxylesterase 2 (CES2) is one of the most important Phase I drug metabolizing enzymes in the carboxylesterase family. It plays crucial roles in the bioavailability of oral ester prodrugs and the therapeutic effect of some anticancer drugs such as irinotecan (CPT11) and capecitabine. In addition to the well-known roles of CES2 in xenobiotic metabolism, the enzyme also participates in endogenous metabolism and the production of lipids. In this study, we synthesized a series of pyrazolones and assayed their inhibitory effects against CES2 in vitro. Structure-activity relationship analysis of these pyrazolones reveals that the introduction of 4-methylphenyl unit ($R^1$), 4-methylbenzyl ($R^2$) and cyclohexyl ($R^3$) moieties are beneficial for CES2 inhibition. Guided by these SARs results, 1-cyclohexyl-4-(4-methylbenzyl)-3-p-tolyl-1H- pyrazol-5(4H)-one (**27**) was designed and synthesized. Further investigations demonstrated that the compound **27** exhibited stronger CES2 inhibition activity with a lower $IC_{50}$ value (0.13 μM). The inhibition kinetic study demonstrated that compound **27** inhibited the hydrolysis of CES2-fluorescein diacetate (FD) through non-competitive inhibition. In addition, the molecular docking showed that the core of pyrazolone, the cyclohexane moiety, 4-methylbenzyl and 4-methylphenyl groups in compound **27** all played important roles with the amino acid residues of CSE2. Also, compound **27** could inhibit adipocyte adipogenesis induced by mouse preadipocytes. In brief, we designed and synthesized a novel pyrazolone compound with a strong inhibitory ability on CES2 and could inhibit the adipogenesis induced by mouse preadipocytes, which can be served as a promising lead compound for the development of more potent pyrazolone-type CES2 inhibitors, and also used as a potential tool for exploring the biological functions of CES2 in human being.

## 1. Introduction

Carboxylesterase (CES, E.C. 3.1.1.1) is a super family with 93 subfamilies.[1] There are two main types of aryl esterases in the human body, namely human carboxylesterase 1 (CES1) and human carboxylesterase 2 (CES2). The CES2 is an esterase mainly distributed in human intestine and colon, which could hydrolyze exogenous compounds containing ester- and amide,[2,3] and metabolize the ester-containing drugs and environmental toxicants. For example, when the prodrug irinotecan (CPT-11) featuring a carbamate was used to treat patients with colorectal cancer, the excessive accumulation of SN-38 (7-Ethyl-10-Hydroxy-camptothecin, the hydrolytic metabolite of irinotecan) could cause severe delayed diarrhea. Increasing evidences have indicated that potent inhibition on intestinal CES2 may reduce the excessive accumulation of SN-38 in the intestinal tract and thereby alleviate the intestinal toxicity triggered by irinotecan.[4] Therefore, the combination of CES2 inhibitors and CPT-11 was considered to be an effective way to relieve the persistent diarrhea.[5–7]

In addition, CES2 also participates in the metabolism of endogenous substances in *vivo*, such as triacylglycerol and diacylglycerol.[8] CES2 expression has a certain correlation in non-alcoholic steatohepatitis and obesity.[9] Despite it was reported that CES2 was a triacylglycerol

---

hydrolase that assumed as a fundamental part in regulating the hepatic triglyceride homeostasis by managing endoplasmic reticulum stress, lipolysis, fatty acid oxidation, and lipogenesis,[10] there were articles showing that knocking out mice's carboxylesterase 3 (Ces3, homologous to human CES1) would cause the decrease of its blood lipids, the improvement of its glucose tolerance and the increase of its energy consumption.[11] Meanwhile, mice's Ces3 activation contributed to the browning of white adipocytes in *vitro*, resulting in the reduction of the fat formation of 3 T3-L1 adipocytes.[12] However, the adipogenic effect of CES2 in 3 T3-L1 adipocytes has not been reported yet. The relationship between CES2 and obesity, diabetes and other diseases are hot research topics. Therefore, the development of CES2 inhibitors are particularly important for the research of metabolic function and the state and development of diseases.[9,13,14]

Pyrazolone is a nitrogen-containing five-membered heterocyclic compound, which is the core structure of many analgesic drugs. For example, antipyrine, propyphenazone and famprofazone.[15] In addition, pyrazolones have a wide range of biological activities in anti-tuberculosis,[16] anti-viral,[17] anti-hypertension,[18] anti-oxidation,[19] neuro-protection,[20] anti-diabetic,[21] anti-inflammatory[22] and anti-cancer.[23] In our previous report, we have developed several highly specific optical substrates that produced fluorescence after hydrolysis of probes. These substrates have been successfully used for high-throughput screening of natural CES2 inhibitors.[24–26] Herein, we designed and synthesized a series of pyrazolone derivatives featuring easily accessible scaffold and a simple two-step protocol. Through the transformation of the substituent-properties of these pyrazolones, we established the structure–activity relationship between CES2 and pyrazolones for the further design and synthesis of more potent CES2 inhibitor. Finally, the use of the CES2 inhibitor to inhibit the formation of fat granules in induced mouse preadipocytes was verified in cells.

## 2. Methods and materials

### 2.1. Reagents and standards

Fluorescein diacetate (FD), loperamide (LPA) and bis-p-nitro-phenyl phosphate (BNPP) were purchased from TCI (Tokyo, Japan). Human liver microsomes (HLM) were obtained from Research Institute for Liver Diseases (RILD, Shanghai, China). Insulin, 3-isobutyl1-methylxanthine were obtained from Sigma (St. Louis, MO, US). Dexamethasone was obtained from ICN BIOMEDICALS INC. (CA, US). Oil red O staining kit was purchased from Solarbio (Beijing, China). All other reagents and fine chemicals with the highest grade were from Sigma, Tedia (Fairfield, OH, USA), and J&K Chemical Ltd. (Shang-hai, China). Substrate and compounds were dissolved in DMSO (Tedia, USA) and stored in re-frigerators at 4 °C until use. All $^1$H NMR and $^{19}$F NMR spectra were recorded on a Bruker Avance II 400 MHz and Bruker Avance III 471 MHz respectively, $^{13}$C NMR spectra were recorded on a Bruker Avance II 101 MHz or Bruker Avance III 126 MHz with chemical shifts reported as ppm (in CDCl$_3$, TMS as internal standard). Data for $^1$H NMR are recorded as follows: chemical shift ($\delta$, ppm), multiplicity (s = singlet, d = doublet, t = triplet, m = multiplet, br = broad singlet, dd = doublet doublet, coupling constants in Hz, integration). HRMS (ESI) was obtained with a HRMS/MS instrument (LTQ Orbitrap XL TM).

### 2.2. The synthesis of pyrazolones derivatives

Pyrazolones **1, 3, 5, 6, 8, 10, 11, 13, 15, 17, 21–24** were prepared according to the literature.[27–29] Pyrazolones **2, 4, 7, 9, 12, 14, 16, 18–20, 25–27** were prepared from the corresponding $\beta$-keto esters **1S** according to the slightly modified procedure from the general procedure.

General procedure: To a 50 mL round-bottom flask was added 10 mL of anhydrous THF and NaH (60% in mineral oil, 0.48 g, 12 mmol) under argon. After cooled to 0 °C, a solution of the corresponding $\beta$-ketone ester **1S** (10 mmol) in 5 mL of anhydrous THF was added dropwise. The resulting mixture was then warmed to rt for 1 h. After cooled to 0 °C, the corresponding alkyl bromide (10 mmol) or alkyl chloride (10 mmol) was added dropwise to the mixture. The mixture was then stirred at rt (for alkyl bromide) or at 70 °C (for alkyl chloride). The reaction process was detected by TLC analysis. After completion, the reaction mixture was cooled to 0 °C, and then quenched by 10 mL of saturated NH$_4$Cl aqueous carefully. The reaction mixture was extracted with ethyl acetate (3 × 10 mL). The combined organic phase was then washed with brine and dried over Na$_2$SO$_4$, concentrated. The crude mono-substituted $\beta$-ketone ester **2S** was used without further purification for next step with quantitive yield.

To a 50 mL round-bottom flask was added mono-substituted $\beta$-ketone ester **2S** (10 mmol) and mono-substituted hydrazine (11 mmol), under argon. The neat mixture was then stirred at 120 °C for 4–6 h. The reaction was detected with TLC analysis. After cooling to rt, the resulting solid was recrystallized with EtOH to yield the final pyrazolone. If no product was precipitated, the mixture was then purified by column chromatography on silica gel with petroleum ether/ethyl acetate as eluent.

The pyrazolones exist in tautomeric forms (ketone form and enol form).[30] So the NMR data was usually showed as a mixture of ketone form and enol form.

4-(4-methylbenzyl)-1,3-diphenyl-1$H$-pyrazol-5(4$H$)-one (**2**) white solid, yield 40%; $^1$H NMR for the enol form (400 MHz, DMSO-$d_6$) $\delta$ 11.14 (s, 1H), 7.95 (d, $J$ = 8.0 Hz, 2H), 7.65 (d, $J$ = 7.2 Hz, 2H), 7.55–7.26 (m, 6H), 7.18–7.04 (m, 4H), 3.97 (s, 1H), 2.25 (s, 3H); $^{13}$C NMR (101 MHz, DMSO-$d_6$) $\delta$ 149.6, 138.3, 135.2, 129.4, 128.9, 128.2, 127.5, 126.1, 121.8, 27.9, 21.1; HRMS (EI) $m/z$ Calcd. for C$_{23}$H$_{20}$N$_2$O ([M]$^+$) 340.1570, Found 340.1577.

4-(2-methylbenzyl)-1,3-diphenyl-1$H$-pyrazol-5(4$H$)-one (**4**) yellow solid, yield 48%; $^1$H NMR for a mixture of ketone form and enol form (400 MHz, CDCl$_3$) $\delta$ 10.07 (s, 1H), 7.94–7.82 (m, 1.6 H$_{ketone}$), 7.52 (d, $J$ = 7.8 Hz, 2H), 7.49–7.44 (m, 1.6 H$_{ketone}$), 7.40–7.34 (m, 2.4H), 7.33–7.28 (m, 1.8H), 7.25–7.17 (m, 8H), 7.09 (t, $J$ = 7.3 Hz, 1H), 7.04–6.92 (m, 6H), 6.89 (d, $J$ = 7.1 Hz, 1H), 3.93–3.84 (m, 0.8H), 3.39 (s, 2H), 3.27 (dd, $J$ = 14.4, 5.9 Hz, 0.8 H$_{ketone}$), 3.20 (dd, $J$ = 14.4, 7.0 Hz, 0.8 H$_{ketone}$)., 2.06 (s, 5.4H); $^{13}$C NMR (101 MHz, CDCl$_3$) $\delta$ 173.2, 159.2, 149.9, 138.1, 138.0, 136.5, 135.9, 134.5, 130.8, 130.5, 130.4, 129.8, 129.7, 129.2, 128.9, 128.7, 128.6, 127.7, 127.2, 126.8, 126.0, 125.9, 125.5, 125.4, 120.6, 119.3, 50.4, 32.7, 25.7, 19.6, 19.50; HRMS (EI) $m/z$ Calcd. for C$_{23}$H$_{20}$N$_2$O ([M]$^+$) 340.1570, Found 340.1566.

4-(4-bromobenzyl)-1,3-diphenyl-1H-pyrazol-5(4$H$)-one (**7**) White solid, yield 50%; $^1$H NMR (400 MHz, DMSO-$d_6$) $\delta$ 11.07 (br. s, 1H), 7.85 (d, $J$ = 8.0 Hz, 2H), 7.56 (d, $J$ = 6.4 Hz, 2H), 7.52–7.42 (m, 4H), 7.42–7.21 (m, 4H), 7.13 (d, $J$ = 7.2 Hz, 2H), 3.92 (s, 2H). $^{13}$C NMR (101 MHz, CDCl$_3$) $\delta$ 172.8, 157.8, 137.8, 134.4, 131.5, 131.0, 130.8, 130.1, 129.3, 129.0, 127.9, 126.6, 125.7, 121.4, 119.6, 50.8, 34.8. HRMS (ESI): calcd. for C$_{22}$H$_{17}$BrN$_2$ONa (M+Na)$^+$ 427.0422 found: 427.0414.

1,3-diphenyl-4-(4-(trifluoromethyl)benzyl)-1$H$-pyrazol-5(4$H$)-one (**9**) white solid, yield 70%; $^1$H NMR for a mixture of ketone form and enol form (400 MHz, CDCl$_3$) $\delta$ 7.78–7.72 (m, 2H), 7.72–7.65 (m, 2H), 7.64–7.55 (m, 1.3H$_{enol}$), 7.54–7.46 (m, 3H), 7.45–7.31 (m, 8.3H), 7.30–7.23 (m, 1.7H), 7.23–7.11 (m, 3H), 7.01 (d, $J$ = 8.1 Hz, 2H), 4.11–4.02 (m, 1H), 3.62 (s, 1.2H$_{enol}$), 3.48 (dd, $J$ = 13.8, 4.5 Hz, 1H), 3.37 (dd, $J$ = 13.8, 5.5 Hz, 1H); $^{19}$F NMR (470 MHz, CDCl$_3$) $\delta$ −62.35, −62.62; $^{13}$C NMR (101 MHz, CDCl$_3$) $\delta$ 172.6, 157.7, 150.0, 144.6, 139.4, 137.6, 130.7, 129.7, 129.5 (q, $J$ = 32.3 Hz), 129.2, 128.9, 128.8, 128.4, 127.7, 126.5, 125.7, 125.2 (q, $J$ = 4.0 Hz), 124.0 (q, $J$ = 272.7 Hz), 120.4, 119.5, 50.6, 35.0, 28.1; HRMS (EI) $m/z$ Calcd. for C$_{23}$H$_{17}$F$_3$N$_2$O ([M]$^+$) 394.1287, Found 394.1283.

4-(naphthalen-1-ylmethyl)-1,3-diphenyl-1$H$-pyrazol-5(4$H$)-one (**12**) light yellow solid, yield 46%; $^1$H NMR for a mixture of ketone form and enol form(400 MHz, CDCl$_3$) $\delta$ 10.35 (s, 1H), 8.01–7.94 (m, 0.6H$_{ketone}$), 7.88–7.69 (m, 3.8H), 7.64 (d, $J$ = 8.3 Hz, 0.6H$_{ketone}$), 7.57 (d, $J$ = 8.2 Hz, 1H), 7.45–7.26 (m, 7.4H), 7.23–6.87 (m, 13.9H), 4.07–4.00 (m,

0.6H$_{ketone}$), 3.83 (dd, $J = 14.4$, 5.3 Hz, 0.6H$_{ketone}$), 3.72 (s, 2H), 3.46 (dd, $J = 14.5$, 7.6 Hz, 0.6H$_{ketone}$); $^{13}$C NMR (101 MHz, CDCl$_3$) $\delta$ 173.2, 159.6, 149.8, 137.9, 135.5, 133.8, 133.7, 132.2, 131.8, 131.5, 130.9, 130.3, 129.1, 128.9, 128.7, 128.6, 128.5, 128.2, 128.1, 127.6, 126.9, 126.7, 126.2, 125.7, 125.6, 125.5, 125.4, 125.0, 124.9, 123.5, 120.8, 119.3, 50.3, 33.2, 25.2; HRMS (EI) *m/z* Calcd. for C$_{26}$H$_{20}$N$_2$O$^+$ ([M]$^+$) 376.1570, Found 376.1581.

4-allyl-1,3-diphenyl-1H-pyrazol-5(4H)-one (**14**) light yellow solid, yield 43%; $^1$H NMR (400 MHz, DMSO-*d$_6$*) $\delta$ 10.82 (br. s, 1H), 7.82 (d, $J = 8.0$ Hz, 2H), 7.68 (d, $J = 7.2$ Hz, 2H), 7.58–7.32 (m, 5H), 7.27 (t, $J = 7.2$ Hz, 1H), 6.06–5.84 (m, 1H), 5.10–4.91 (m, 2H), 3.30 (m, 2H). $^{13}$C NMR (101 MHz, DMSO-*d$_6$*) $\delta$ 149.1, 138.6, 137.0, 134.2, 128.9, 128.5, 127.1, 125.7, 121.3, 114.9, 97.7, 26.3. HRMS (ESI): calcd. for C$_{18}$H$_{16}$N$_2$ONa (M+Na)$^+$ 299.1160 found: 299.1168.

4-benzyl-3-(4-bromophenyl)-1-phenyl-1H-pyrazol-5(4H)-one (**16**) white solid, yield 65%; $^1$H NMR for the enol form(400 MHz, DMSO-*d$_6$*) $\delta$ 11.16 (s, 1H), 7.87 (d, $J = 7.9$ Hz, 2H), 7.67–7.44 (m, 6H), 7.36–7.09 (m, 6H), 3.99 (s, 2H); $^{13}$C NMR (400 MHz, DMSO-*d$_6$*) $\delta$ 151.0, 148.3, 141.2, 131.8, 129.4, 128.8, 128.3, 126.3, 121.9, 28.1; HRMS (ESI): calcd. for C$_{22}$H$_{17}$BrN$_2$NaO$^+$ ([M+Na]$^+$) 427.0416, found 427.0409.

4-benzyl-1-phenyl-3-p-tolyl-1H-pyrazol-5(4H)-one (**18**) white solid, yield 55%; $^1$H NMR for the enol form(400 MHz, DMSO-*d$_6$*) $\delta$ 11.01 (s, 1H), 7.88 (d, $J = 7.1$ Hz, 2H), 7.50 (t, $J = 7.7$ Hz, 4H), 7.30–7.11 (m, 8H), 3.99 (s, 2H), 2.30 (s, 3H); $^{13}$C NMR (400 MHz, DMSO-*d$_6$*) $\delta$ 151.5, 149.5, 141.4, 139.3, 129.4, 128.8, 128.3, 127.3, 126.2, 121.8, 98.8, 28.2, 21.3; HRMS (ESI): calcd. for C$_{23}$H$_{21}$N$_2$O ([M+H]$^+$) 341.1648, found 341.1636.

341.1648

4-benzyl-1-phenyl-3-m-tolyl-1H-pyrazol-5(4H)-one (**19**) white solid, yield 48%; $^1$H NMR for the enol form(400 MHz, DMSO-*d$_6$*) $\delta$ 11.05 (s, 1H), 7.88 (d, $J = 7.3$ Hz, 2H), 7.50 (t, $J = 7.8$ Hz, 2H), 7.44–7.07 (m, 10*H*), 3.99 (s, 2H), 2.27 (s, 3H); $^{13}$C NMR (400 MHz, DMSO-*d$_6$*) $\delta$ 151.5, 149.6, 141.6, 137.8, 134.5, 129.4, 128.8, 128.3, 128.1, 126.3, 124.5, 121.9, 119.1, 99.1, 28.3, 21.5; HRMS (ESI): calcd. for C$_{23}$H$_{21}$N$_2$O ([M+H]$^+$) 341.1648, found 341.1641.

4-benzyl-1-phenyl-3-(thiophen-2-yl)-1H-pyrazol-5(4H)-one (**20**) white solid, yield 56%; $^1$H NMR for the enol form(400 MHz, DMSO-*d$_6$*) $\delta$ 11.18 (s, 1H), 7.87 (d, $J = 8.0$ Hz, 2H), 7.56–7.35 (m, 4H), 7.32–7.16 (m, 4H), 7.13–6.99 (m, 3H), 3.85 (s, 2H); $^{13}$C NMR (101 MHz, DMSO-*d$_6$*) $\delta$ 144.7, 140.9, 139.0, 129.4, 128.8, 128.1, 126.3, 121.8, 28.1; HRMS (EI) *m/z* Calcd. for C$_{20}$H$_{14}$N$_2$OS ([M−H$_2$]$^+$) 330.0821, Found 330.0832.

4-benzyl-1-methyl-3-phenyl-1H-pyrazol-5(4H)-one (**25**) light yellow solid, yield 54%; $^1$H NMR for a mixture of ketone form and enol form (400 MHz, CDCl$_3$) $\delta$ 8.03–7.98 (m, 1.7H), 7.55 (dd, $J = 6.6$, 3.1 Hz, 1.3H), 7.44–7.38 (m, 4.5H), 7.33 (dd, $J = 7.5$, 1.8 Hz, 2.1H), 7.25–7.20 (m, 2.7H), 7.14–7.03 (m, 9.6H), 6.85–6.78 (m, 2.8H), 3.79 (t, $J = 5.1$ Hz, 0.6H$_{ketone}$), 3.64 (s, 2H), 3.32 (d, $J = 1.1$ Hz, 1.8H$_{ketone \, and \, enol}$), 3.28 (d, $J = 4.8$ Hz, 0.6H$_{ketone}$), 3.21 (s, 3H), 3.15 (s, 1.8H$_{ketone}$), 2.99 (s, 2.4H$_{enol}$); $^{13}$C NMR (101 MHz, CDCl$_3$) $\delta$ 175.3, 174.5, 160.9, 157.9, 157.8, 146.6, 140.8, 135.4, 132.5, 131.1, 130.5, 130.4, 130.2, 129.7, 129.1, 129.0, 128.8, 128.6, 128.3, 128.1, 128.0, 127.9, 127.7, 127.3, 127.1, 126.7, 126.3, 125.8, 102.5, 81.0, 49.6, 44.2, 35.1, 31.2, 31.1, 30.9, 28.2; HRMS (EI) *m/z* Calcd. for C$_{17}$H$_{16}$N$_2$O$^+$ ([M]$^+$) 264.1257, Found 264.1268.

4-benzyl-1-cyclohexyl-3-phenyl-1H-pyrazol-5(4H)-one (**26**) white solid, yield 44%; $^1$H NMR for a mixture of ketone form and enol form (400 MHz, DMSO-*d$_6$*) $\delta$10.26 (s, 1H), 7.48 (d, $J = 6.7$ Hz, 2H), 7.33–7.07 (m, 8H), 4.17 (brs, 1H), 3.91 (s, 2H), 1.95–1.80 (m, 6H), 1.67 (d, $J = 11.1$ Hz, 1H), 1.45–1.34 (m, 2H), 1.25–1.15 (dd, $J = 18.5$, 10.8 Hz, 1H); $^{13}$C NMR (101 MHz, DMSO-*d$_6$*) $\delta$ 150.1, 146.8, 142.0, 135.5, 128.7, 128.6, 128.2, 127.2, 127.0, 126.1, 96.8, 55.0, 32.6, 28.3, 25.6, 25.5; HRMS (EI) *m/z* Calcd. for C$_{22}$H$_{24}$N$_2$O ([M]$^+$) 332.1883, Found 332.1896.

1-cyclohexyl-4-(4-methylbenzyl)-3-p-tolyl-1H-pyrazol-5(4H)-one (**27**) white foam, yield 45%; $^1$H NMR for the enol form(400 MHz, DMSO-*d$_6$*) $\delta$10.16 (s, 1H), 7.37 (d, $J = 8.1$ Hz, 2H), 7.10–6.98 (m, 6H), 4.20–4.09 (m, 1H), 3.82 (s, 2H), 2.27 (s, 3H), 2.23 (s, 3H), 1.90–1.77 (m, 6H), 1.67 (d, $J = 12.6$ Hz, 1H), 1.42–1.33 (m, 2H), 1.27–1.18 (m, 1H); $^{13}$C NMR (400 MHz, DMSO-*d$_6$*) $\delta$ 150.10, 146.8, 138.93, 136.5, 134.8, 129.8, 129.2, 128.7, 128.1, 126.9, 126.4, 96.8, 55.1, 32.5, 27.9, 25.7, 25.5, 21.2, 21.0; HRMS (ESI): calcd. for C$_{24}$H$_{29}$N$_2$O ([M+H]$^+$) 361.2274, found 361.2288.

## 2.3. CES2 inhibitor screening method

The CES 2 inhibitor screening method refers to the previously reported FD as substrate to produce fluorescence product after being hydrolyzed. The reaction consists of the following materials: phosphate buffer (194 μL 50 mM, pH 7.4), CES2 enzyme source (2 μL, final concentration 20 μg/mL HLM) and the compound to be screened (2 μL, dissolved in DMSO) were suspended in an EP tube, and then pre-incubated at 37℃ for 3 mins. The substrate FD (2 μL, dissolved in DMSO final concentration 50 μM) was added to initiate the reaction. After 20 mins, the same volume of acetonitrile (200 μL) was added to terminate the reaction. Finally, 200 mL of the mixture was added to the microplate. Put it into the microplate reader for detection at excitation wavelength/emission wavelength = 495/520 nm.

## 2.4. Statistical analysis

The calculation methods of half-maximal inhibitory concentration (IC$_{50}$) and inhibition kinetics are as previously reported.[31] The residual activities of CES2 were calculated using the following formula: the residual activity (%) = (the florescence intensity in the presence of inhibitor)/the florescence intensity in negative control (DMSO only) 100%. Different inhibitor concentrations were used to determine IC$_{50}$ of each compound by Inhibition log(inhibitor) vs. normalized response using GraphPad Prism 6.0 software. In order to determine the type of inhibition kinetics (mixed inhibition, non-competitive inhibition or competitive inhibition), multiple substrate concentrations and various inhibitor concentrations can be used to determine the corresponding reaction rate. The second plot from the slope of the Lineweaver-Burk plot is used as a function of [inhibitor] to calculate the corresponding inhibition constant (Ki) value. Data are expressed as mean ± SD.

## 2.5. Molecular docking

The 3D structure of CES2 was downloaded from the SWISS-MODEL library (a database of annotated 3D protein structure models generated by homology modeling pipeline), and the accession number is O00748.[32] The docking protocol of CES2 and ligand was as reported in the previous article.[33] Molecular docking was performed using Auto-Dock Vina version 1.1.2.[34] The crystallized waters were removed, and the protein was assigned polar hydrogens and united atom Kollman charges. The docking grid was generated with a volume of 80 × 80 × 80 and centered at the catalytic triad (Ser228, Glu345, and His457).[2] The docking simulation was carried out based on the Lamarckian genetic algorithm. The protein–ligand pose with the lowest binding energy was displayed in full text.

## 2.6. Cell culture

Caco-2 (ATCC HTB-37, Manassas, VA, USA) and HepG2 (ATCC HB-8065, Manassas, VA, USA) cells were cultured in GibcoDulbecco's Modified Eagle medium (DMEM), supplemented with 10% fetal bovine serum (FBS, Gibco, US), and 1% penicillin–streptomycin (Dalian Meilun Biotechnology Co., Ltd., Dalian, China) at 37℃ with 5% CO$_2$.[35] 3 T3-L1 cells (ATCC CL-173, Manassas, VA, USA) were cultured in Gibco-Dulbecco's Modified Eagle Medium/F:12 (DMEM/F:12), supplemented with 10% FBS, and 1% penicillin–streptomycin at 37℃ with 5% CO$_2$. The method of 3 T3-L1 cells differentiation into adipocytes was improved on the basis of previous reports.[36] The cells were planted in a

well plate and cultured for 48 h after the cells were 100% confluent. The CES2 inhibitors were mixed with solution I (10 µg/mL insulin, 0.5 mM 3-isobutyl −1- methylxanthine, and 1 mM dexamethasone dissolved in DMEM/F:12 medium) to different concentrations, then added to different wells and incubated for 48 h Subsequently, the CES2 inhibitors were mixed with solution II (10 µg/mL insulin dissolved in DMEM/F:12 medium) at different concentrations, and then added to the wells of the same concentration and incubated for 48 h. Afterwards, the medium in the wells were replaced with DMEM/F:12 medium with different concentrations of CES2 inhibitors and continued to be cultured for 48 h.

### 2.7. Cytotoxicity assays

Cell viability was investigated by CCK-8 Kit ((Dalian Meilun Biotechnology Co., Ltd., Dalian, China)). 3 T3-L1, Caco-2,HepG2 cells (5 × $10^4$/mL, 200 µL) were seeded in the 96-well plate and maintained at 37℃ in a 5% $CO_2$ incubator for 24 h. Then the cells were incubated with different concentrations of compound **27** (0–100 µM) for another 48 h. CCK-8 (10%, w/v, 100 µL) was added into the adherent cells and fixed in 37℃ for 2 h. The absorbance was measured at 450 nm.

### 2.8. Oil red O staining

After the above-mentioned adipocytes were cultured for 48 h. 3 T3-L1 cells were washed with PBS and fixed for 20–30 mins at room temperature, and then washed again with deionized water for 3 times. Added 60% isopropanol and washed for 5 mins. The oil red O solution was soaked in the wells for 20 mins, then washed with deionized water 3 times. Added hematoxylin staining solution to stain the nucleus for 2 mins, and finally added deionized water to observe the stained lipid droplets under an inverted microscope (Echo Laboratories RevolveFL).

### 3. Results

#### 3.1. Synthesis of pyrazolones derivatives

A series of pyrazolone compounds were synthesized by a simple two-step process, as shown in Table 1. Derivatives with different $R^1$, $R^2$ and $R^3$ were labeled as compounds **1**–**27**. The synthetic route was shown in Fig. 1. See materials and methods for specific synthetic methods.

#### 3.2. CES2 inhibition of pyrazolone derivatives

In the previous works, we screened a series of polycyclic compounds for CES2 inhibitory activity, such as triterpenes and bis(indolyl)methane derivatives.[24–26,33,37] And tried to explain the relationship between the modification of different sites on the original nucleus and the inhibition of CES2. In this study, we performed CES2 activity inhibition screening on twenty-seven pyrazolone derivatives and measured all the half inhibitory concentration (IC$_{50}$), which were listed in Table 1.

#### 3.3. SAR analysis of pyrazolones derivatives

We modified the pyrazolones at positions C3, C4 and N1, which were showed as $R^1$, $R^2$, and $R^3$, respectively. Combining the results of their inhibitions to CES2, the structure–activity relationship could be derived. Compounds **1**–**14** had the same $R^1$ and $R^3$ (phenyl group). When $R^2$ were 4-methylbenzyl, 3-methylbenzyl, 4-methoxylbenzyl, 4-bromobenzyl, ethyl, or allyl groups, these pyrazolones showed IC$_{50}$ values against CES2 less than 10 µM (Table 1). Among them, compound **2** with 4-methylbenzyl unit showed the best inhibitory effect against CES2 with IC$_{50}$ value of 5.16 µM. Compounds **15**–**21** were substituted with benzyl and phenyl at the C4 and N1 positions, respectively. Further characterizations of compounds **15**–**21** with the variation of $R^1$ unit demonstrated that compound **18** with 4-methylphenyl substitute was more beneficial for inhibitory property towards CES2 with IC$_{50}$ value of 3.82 µM. The

**Table 1**
The IC$_{50}$ values of pyrazolones derivatives toward CES2.

| Compound | $R^1$ | $R^2$ | $R^3$ | IC$_{50}$ (µM) |
|---|---|---|---|---|
| **1** | Ph | Bn | Ph | 12.19 ± 1.29 |
| **2** | Ph | 4-methylbenzyl | Ph | 5.16 ± 0.43 |
| **3** | Ph | 3-methylbenzyl | Ph | 7.11 ± 1.75 |
| **4** | Ph | 2-methylbenzyl | Ph | 23.25 ± 3.92 |
| **5** | Ph | 4-methoxylbenzyl, | Ph | 6.68 ± 1.10 |
| **6** | Ph | 4-fluorobenzyl | Ph | 19.40 ± 3.64 |
| **7** | Ph | 4-bromobenzyl | Ph | 8.24 ± 0.68 |
| **8** | Ph | 2-chlorobenzyl | Ph | 23.70 ± 4.15 |
| **9** | Ph | 4-trifluoromethyl-benzyl | Ph | 17.01 ± 4.12 |
| **10** | Ph | 3,5-ditrifluoromethyl-benzyl | Ph | 14.29 ± 3.97 |
| **11** | Ph | 2- nitrobenzyl | Ph | 10.90 ± 1.40 |
| **12** | Ph | 1-naphthyl methyl | Ph | 22.35 ± 9.48 |
| **13** | Ph | ethyl | Ph | 9.04 ± 2.23 |
| **14** | Ph | allyl | Ph | 7.76 ± 1.91 |
| **15** | 4-methoxylphenyl | Bn | Ph | 15.06 ± 2.81 |
| **16** | 4-bromophenyl | Bn | Ph | 6.19 ± 0.66 |
| **17** | 2-fluorobenzyl | Bn | Ph | 13.00 ± 3.05 |
| **18** | 4-methylphenyl | Bn | Ph | 3.82 ± 0.84 |
| **19** | 3-methylphenyl | Bn | Ph | 11.17 ± 2.10 |
| **20** | 2-thienyl | Bn | Ph | 14.09 ± 3.41 |
| **21** | methyl | Bn | Ph | 38.13 ± 9.40 |
| **22** | methyl | 2-methylbenzyl | Ph | 46.46 ± 12.10 |
| **23** | methyl | 2-chlorobenzyl | Ph | 78.20 ± 13.69 |
| **24** | ethyl | Bn | Ph | 24.87 ± 7.43 |
| **25** | Ph | Bn | methyl | 50.90 ± 15.27 |
| **26** | Ph | Bn | cyclohexyl | 9.12 ± 2.81 |
| **27** | 4-methylphenyl | 4-methylbenzyl | cyclohexyl | 0.13 ± 0.01 |
| **BNPP**[a] | | | | 6.40 ± 1.20 |
| **LPA**[a] | | | | 1.57 ± 0.22 |

[a] Positive inhibitor against CES.

variation of the phenyl group ($R^1$) to methyl or ethyl (compounds **22**–**24**) group finally resulted in a loss of potency (Table 1). Compound **25** with methyl substitute ($R^3$) displayed poor inhibition toward CES2 than compound **1** ($R^3$, Ph), however, the variation of the methyl unit to cyclohexyl unit (compound **26**) finally resulted in a significant increase of potency (IC$_{50}$, 9.12 µM). To summarize the above SAR of these compounds, 4-methylphenyl unit ($R^1$), 4-methylbenzyl ($R^2$) and cyclohexyl ($R^3$) moiety were beneficial for pyrazolone's inhibitory property toward CES2, resulting in a dramatic increase of the inhibitory effect on CES2. Guided by these SARs results, we synthesized a new compound **27**
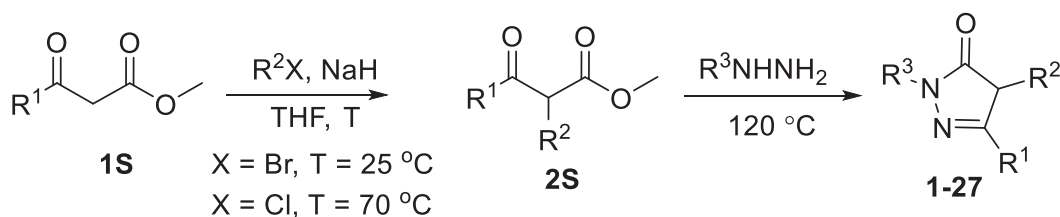
**Fig. 1.** Chemical structures and synthetic route of pyrazolone.

with 4-methylphenyl ($R^1$), 4-methylbenzyl ($R^2$), and cyclohexyl ($R^3$) unit. This novel compound **27** showed potent inhibitory activity against CES2 with the $IC_{50}$ value of 0.13 μM (Fig. 2a). Compared with the $IC_{50}$ values of CES2′s positive inhibitors BNPP and LAP, which were 6.40 μM and 1.57 μM, respectively, the $IC_{50}$ value of compound **27** were about 10 to 60 times lower than the aforementioned two positive inhibitors.

### 3.4. Inhibition kinetic analyses

The strong inhibitory ability of compound **27** on CES2 prompted us to further study the inhibitory mechanism of this pyrazolone derivative on CES2. As shown in Fig. 2b-c, the enzymatic kinetics of FD, Michaelis-Menten equations, and linewever-burk diagram showed that compound **27** inhibited CES2 activity with $K$i value of 0.09 μM. The results showed that the type of inhibition of compound **27** was non-competitive inhibition, which had a quite prominent ability to inhibit CES2 activity.

### 3.5. Docking simulation of compound 27 into human CES2

In order to explore the interaction mode between compound **27** and CES2, molecular docking was simulated. The pyrazolones exist in tautomeric forms (keto form and enol form) (Chauhan et al., 2015). So the ligand **27** position of the enol form and keto form with the lowest binding energy in the CES2 complex were shown in Fig. 3 and Fig. S2, respectively. When compound **27** core existed in enol form, the binding energy of compound **27** on CES2′s catalytic cavity was lower than that of FD on CES2 (-9.1 kcal/mol VS −8.9 kcal/mol), indicating that the binding energy of compound **27** on CES2′s catalytic cavity was more stable than FD. Compound **27** could interact well with the active cavity of CES2, and the main interaction was hydrophobic. Residue Ala150 located at the bottom of the gorge could form an σ-π interaction with the core of pyrazolone and form alkyl-π interaction with 4-methylphenyl group ($R^1$), 4-methylbenzyl group ($R^2$) and the cyclohexane group ($R^3$). Also, Met354 near the entrance of the gorge could form a sulfur-π interaction with the 4-methylphenyl group ($R^1$). The His457 could form cation-π with 4-methylbenzyl group ($R^2$). When compound **27** core was in the form of keto, its binding energy with CES2 (−8.6 kcal/mol) was slightly larger than that of FD, as shown in Fig. 3 and Fig. S2. The cyclohexane group ($R^3$) of compound **27** penetrates into the active cavity to form alkyl-π conjugates with multiple amino acids (Val353,
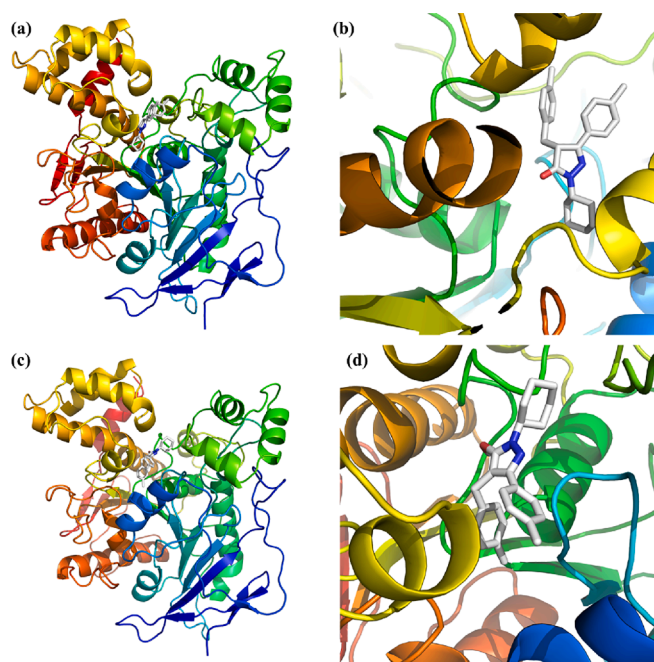


**Fig 3.** (a) CES2 structure and stereogram of compound **27** (enol form); (b) Detailed view of compound **27** (enol form) in the active site of CES2. (c) CES2 structure and stereogram of compound **27** (keto form); (d) Detailed view of compound **27** (keto form) in the active site of CES2.

His457, Phe106 and Ile350 residues). Meanwhile, the Ala150 residue could simultaneously form two alkyl-π interaction with the cyclohexane group ($R^3$) and the 4-methylbenzyl group ($R^2$). Both Met309 and Leu262 residues formed alkyl-π interaction with the 4-methylbenzyl group ($R^2$). Similarly, the Met354 formed alkyl-π, σ-π, sulfur-π interaction with the 4-methylphenyl group ($R^1$). The molecular docking results indicated that two tautomeric forms of compound **27** had a stronger binding ability with the active cavity of CES2 than that of FD, the pyrazolone core of enol form **27** could form an σ-π interaction with the residue Ala150 of CES2 located at the bottom of the gorge, and the cyclohexane group ($R^3$) of keto form **27** penetrates into the active cavity to form
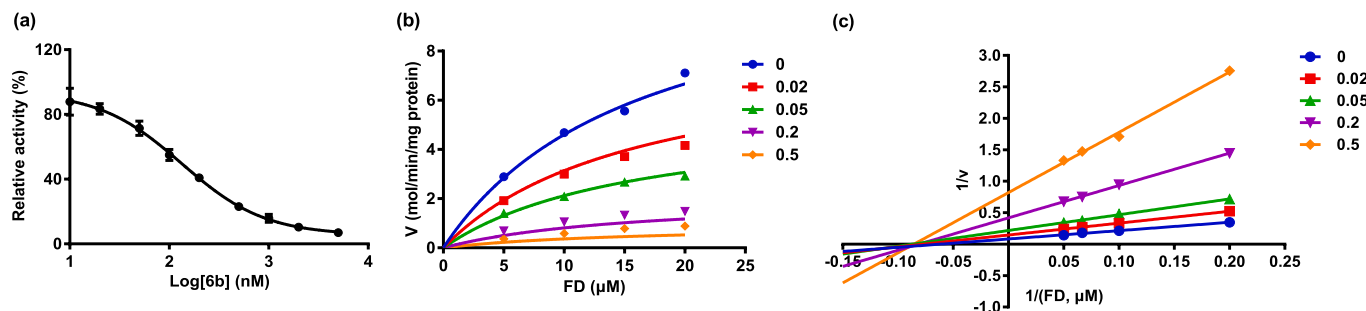


**Fig. 2.** (a) The log(inhibitor) vs. normalized response of **27**; (b) Enzymatic kinetics of FD and Michaelis-Menten equation; (c) The Lineweave-Burk plot of **27** against CES2-mediated FD.

multiple amino acids alkyl-π conjugates.

### 3.6. Pyrazolones inhibit the formation of lipid droplets in 3 T3-L1 cells

In order to study the effect of CES2 inhibitors on the formation of lipid droplets during the induction of mouse preadipocytes 3 T3-L1 into adipocytes, compound **27** was added for pretreatment before cell induction. The results of the cell viability test showed that compound **27** had almost no toxicity to 3 T3-L1, Caco-2 and HepG2 below 40 μM, as shown in Fig. S3. We formulated compound **27**, which was the strongest inhibitor of CES2, into different concentrations and mixed with an inducing agent that induces adipocyte differentiation, and incubated with the cells for 72 h. The cells were stained with oil red O dye after culturing with compound **27** in normal medium for 48 h. The results showed that the lipid droplets in the induced 3 T3-L1 cells (Fig. 4a) were significantly higher than those in the uninduced control group (Fig. 4b). However, there was almost no formation of lipid droplets in the cells treated with compound **27** of high concentration (40 μM). The formation of lipid droplets in cells treated with low concentration (10 μM) was similar to that of the uninduced control. It could be seen from the Fig. 4c-f that the content of lipid droplets of compound **27** gradually increased from high concentration to low concentration. The results indicated that CES2 inhibitors may inhibit the formation of lipid droplets in adipocytes induced by preadipocytes.

## 4. Discussion

The results indicated that pyrazolone compounds exhibited an inhibitory effect on CES2. By comparing the inhibitory activity of a series of compounds on CES2, we found that compound **27** has a strong inhibitory effect on CES2. The discovery and use of pyrazolone compounds provides a new way of thinking, as well as the treatment of metabolic toxicity caused by CES2 provide a more effective drug candidates or lead compounds.

A large number of drugs were purposely or accidentally designed as prodrugs, which could be hydrolyzed by CES2.[38] For example, although the metabolism of CPT-11 in the human body might be mainly participated by P450 enzymes, the metabolite of CES2 was the main structure that exerts its efficacy.[39] Especially in the intestine, the activity of CES2 was the highest relative to other organs. Mass production of SN-38 could cause delayed diarrhea. Therefore, the most effective way was to alleviate the hydrolysis rate of CPT-11 by inhibiting the activity of CES2 in the intestine. According to our results, compound **27** might be a potential treatment drug for persistent diarrhea caused by CPT-11. The results showed that compound **27** inhibited the hydrolysis of FD through non-competitive inhibition. The hydrolysis of CPT-11 might be similar to FD, and it also inhibit the production of SN-38 through non-competitive inhibition. The advantage of this type of inhibition was that it could prevent compound **27** from inhibiting product production by competing with the substrate. $V_{max}$ becomes smaller but $k_m$ remains unchanged, which only affects the amount of product produced without affecting the structure of the enzyme.[40] The docking results also verified the intermolecular interaction between compound **27** and amino acid residues of CES2. The results showed that compound **27** might have tautomerism, and the two forms of structure have strong interactions with CES2. Although compound **27** could dock in the active cavity, they do not interact with Ser228 and Glu345 in the active cavity triplet. This was also consistent with the non-competitive inhibition of compound **27** and the substrate. There is also a possibility that CES2 does not have a crystal structure and can only be docked by homology modeling, which means that there may be other potential sites that interact better with compound **27** and affect the conformation and activity of the active cavity.[41]

Compounds may have multiple effects in the human body.[42] The highly homologous enzyme CES1 has been reported to increase adipogenesis and weaken lipogenesis after been activated. Inhibition of CES1
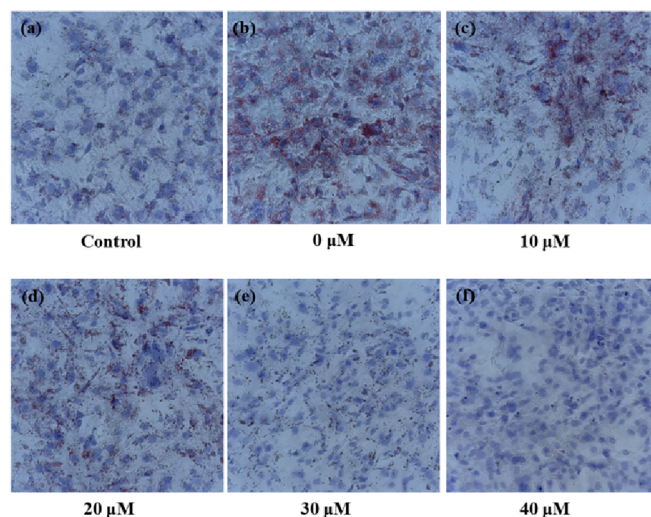


**Fig. 4.** Oil red O staining results of 3 T3-L1 cells (a) normally cultured and (b-f) differentiation culture treated with compound **27** (0–40 μM) (magnification, 20×).

will increase the differentiation of adipocytes and reduce the fat production. Inhibition of CES1 increased fat production.[12] Different from CES2, the above research results showed that CES2 inhibitors could also inhibit adipogenesis and lipogenesis. This might be related to the fact that CES1 was more involved in the metabolism of endogenous fatty acids, while CES2 was less involved in endogenous metabolism. This also indicated that compound **27** may inhibit adipogenesis and lipogenesis through the inhibition of CES2 or other metabolic mechanisms.

In summary, through the SAR analysis of the inhibitory effects of synthesized pyrazolones against CES2, a novel pyrazolone **27** featuring 4-Methylphenyl ($R^1$), 4-methylbenzyl ($R^2$), and cyclohexyl ($R^3$) moieties was designed and synthesized. This new molecule had the best inhibitory effect on CES2 *via* a non-competitive manner with IC$_{50}$ value of 0.13 μM. In addition, the molecular docking showed that the core of pyrazolone, the cyclohexane group ($R^3$), 4-methylbenzyl group ($R^2$), and the 4-methylphenyl group ($R^1$) in compound **27** all played important roles with the amino acid residues of CSE2. The property of **27** to inhibit the formation of intracellular lipid droplets was also confirmed by the mouse preadipocyte induction experiments, which may explained by the obstruction of intracellular adipogenesis after inhibiting CES2. Thus, this new molecule can be served as a promising lead compound for the medicinal chemists to design and develop more efficacious CES2 inhibitors and a potential tool for the biologists to explore the biological functions of CES2 in human being.

## Declaration of Competing Interest

The authors declare that they have no known competing financial interests or personal relationships that could have appeared to influence the work reported in this paper.

## Appendix A. Supplementary material

Supplementary data to this article can be found online at https://doi.

org/10.1016/j.bmc.2021.116187.

# References

1 Long JZ, Cravatt BF. The metabolic serine hydrolases and their functions in mammalian physiology and disease. *Chem Rev*. 2011;111:6022–6063.

2 Wang D, Zou L, Jin Q, Hou J, Ge G, Yang L. Human carboxylesterases: a comprehensive review. *Acta pharmaceutica Sinica. B*. 2018;8:699–712.

3 Laizure SC, Herring V, Hu Z, Witbrodt K, Parker RB. The role of human carboxylesterases in drug metabolism: have we overlooked their importance? *Pharmacotherapy*. 2013;33:210–222.

4 Xu G, Zhang W, Ma MK, McLeod HL. Human carboxylesterase 2 is commonly expressed in tumor tissue and is correlated with activation of irinotecan. *Clin Cancer Res: Off J Am Assoc Cancer Res*. 2002;8:2605–2611.

5 Wang DD, Jin Q, Hou J, et al. Highly sensitive and selective detection of human carboxylesterase 1 activity by liquid chromatography with fluorescence detection. *J Chromatogr B, Anal Technol Biomed Life Sci*. 2016;1008:212–218.

6 Wang DD, Zou LW, Jin Q, Hou J, Ge GB, Yang L. Recent progress in the discovery of natural inhibitors against human carboxylesterases. *Fitoterapia*. 2017;117:84–95.

7 Zou LW, Jin Q, Wang DD, et al. Carboxylesterase inhibitors: an update. *Curr Med Chem*. 2018;25:1627–1649.

8 Ross MK, Crow JA. Human carboxylesterases and their role in xenobiotic and endobiotic metabolism. *J Biochem Mol Toxicol*. 2007;21:187–196.

9 Ruby MA, Massart J, Hunerdosse DM, et al. Human carboxylesterase 2 reverses obesity-induced diacylglycerol accumulation and glucose intolerance. *Cell reports*. 2017;18:636–646.

10 Li Y, Zalzala M, Jadhav K, et al. Carboxylesterase 2 prevents liver steatosis by modulating lipolysis, endoplasmic reticulum stress, and lipogenesis and is regulated by hepatocyte nuclear factor 4 alpha in mice. *Hepatology*. 2016;63:1860–1874.

11 Wei E, Ben Ali Y, Lyon J, et al. Loss of TGH/Ces3 in mice decreases blood lipids, improves glucose tolerance, and increases energy expenditure. *Cell Metab*. 2010;11:183–193.

12 Mukherjee S, Choi M, Yun JW. Novel regulatory roles of carboxylesterase 3 in lipid metabolism and browning in 3T3-L1 white adipocytes. *Appl Physiol Nutrit Metab = Physiologie appliquee, nutrition et metabolisme*. 2019;44:1089–1098.

13 Li B, Cheng Y, Yu S, et al. Human umbilical cord-derived mesenchymal stem cell therapy ameliorates nonalcoholic fatty liver disease in obese type 2 diabetic mice. *Stem Cells Int*. 2019;2019:8628027.

14 Tian X, Yan F, Zheng J, et al. Endoplasmic reticulum targeting ratiometric fluorescent probe for carboxylesterase 2 detection in drug-induced acute liver injury. *Anal Chem*. 2019;91:15840–15845.

15 Levy M. Hypersensitivity to pyrazolones. *Thorax*. 2000;55(Suppl 2):S72–74.

16 Sweeney NL, Lipker L, Hanson AM, et al. Docking into mycobacterium tuberculosis thioredoxin reductase protein yields pyrazolone lead molecules for methicillin-resistant Staphylococcus aureus. *Antibiotics*. 2017;6.

17 Ramajayam R, Tan KP, Liu HG, Liang PH. Synthesis and evaluation of pyrazolone compounds as SARS-coronavirus 3C-like protease inhibitors. *Bioorg Med Chem*. 2010;18:7849–7854.

18 Hassan MQ, Akhtar MS, Afzal O, et al. Edaravone and benidipine protect myocardial damage by regulating mitochondrial stress, apoptosis signalling and cardiac biomarkers against doxorubicin-induced cardiotoxicity. *Clin Exp Hypertens*. 2020;42:381–392.

19 Bailly C. Potential use of edaravone to reduce specific side effects of chemo-, radio- and immuno-therapy of cancers. *Int Immunopharmacol*. 2019;77, 105967.

20 Bhandari R, Kuhad A, Kuhad A. Edaravone: a new hope for deadly amyotrophic lateral sclerosis. *Drugs Today*. 2018;54:349–360.

21 Haroun M. Novel hybrids of pyrazolidinedione and benzothiazole as TZD analogues. Rationale design, synthesis and in vivo anti-diabetic evaluation. *Med Chem*. 2019;15:624–633.

22 Abdelgawad MA, Labib MB, Ali WAM, Kamel G, Azouz AA, El-Nahass ES. Design, synthesis, analgesic, anti-inflammatory activity of novel pyrazolones possessing aminosulfonyl pharmacophore as inhibitors of COX-2/5-LOX enzymes: Histopathological and docking studies. *Bioorg Chem*. 2018;78:103–114.

23 Sun X, Zhang L, Gao M, et al. Nanoformulation of a novel pyrano[2,3-c] pyrazole heterocyclic compound AMDPC exhibits anti-cancer activity via blocking the cell cycle through a P53-independent pathway. *Molecules*. 2019;24.

24 Bao X, Wei S, Qian X, et al. Asymmetric construction of a multi-pharmacophore-containing dispirotriheterocyclic scaffold and identification of a human carboxylesterase 1 inhibitor. *Org Lett*. 2018;20:3394–3398.

25 Zou LW, Li YG, Wang P, et al. Design, synthesis, and structure-activity relationship study of glycyrrhetinic acid derivatives as potent and selective inhibitors against human carboxylesterase 2. *Eur J Med Chem*. 2016;112:280–288.

26 Zou LW, Dou TY, Wang P, et al. Structure-activity relationships of pentacyclic triterpenoids as potent and selective inhibitors against human carboxylesterase 1. *Front Pharmacol*. 2017;8:435.

27 Gagnon PE, Boivin JL, Paquin RJ. Synthesis, potentiometric titrations, and spectra of pyrazolones. *Can J Chem*. 1953;31:1025–1039.

28 Liao YH, Chen WB, Wu ZJ, et al. Organocatalytic asymmetric michael addition of pyrazolin-5-ones to nitroolefins with bifunctional thiourea: stereocontrolled construction of contiguous quaternary and tertiary stereocenters. *Adv Synth Catal*. 2010;352:827–832.

29 Wang Z, Yang ZG, Chen DH, Liu XH, Lin LL, Feng XM. Highly enantioselective michael addition of pyrazolin-5-ones catalyzed by chiral metal/N, N '-dioxide complexes: metal-directed switch in enantioselectivity. *Angew Chem-Int Ed*. 2011;50:4928–4932.

30 Chauhan P, Mahajan S, Enders D. Asymmetric synthesis of pyrazoles and pyrazolones employing the reactivity of pyrazolin-5-one derivatives. *Chem Commun*. 2015;51:12890–12907.

31 Weng ZM, Ge GB, Dou TY, et al. Characterization and structure-activity relationship studies of flavonoids as inhibitors against human carboxylesterase 2. *Bioorg Chem*. 2018;77:320–329.

32 Waterhouse A, Bertoni M, Bienert S, et al. SWISS-MODEL: homology modelling of protein structures and complexes. *Nucleic Acids Res*. 2018;46:W296–W303.

33 Zhao Y-S, Ruan H-L, Wang X-Y, et al. Catalyst-free visible-light-induced condensation to synthesize bis(indolyl)methanes and biological activity evaluation of them as potent human carboxylesterase 2 inhibitors. *RSC Adv*. 2019;9:40168–40175.

34 Wang Z, Sun HY, Yao XJ, et al. Comprehensive evaluation of ten docking programs on a diverse set of protein-ligand complexes: the prediction accuracy of sampling power and scoring power. *PCCP*. 2016;18:12964–12975.

35 Xue L, Qian X, Jin Q, et al. Construction and application of a high-content analysis for identifying human carboxylesterase 2 inhibitors in living cell system. *Anal Bioanal Chem*. 2020;412:2645–2654.

36 Zebisch K, Voigt V, Wabitsch M, Brandsch M. Protocol for effective differentiation of 3T3-L1 cells to adipocytes. *Anal Biochem*. 2012;425:88–90.

37 Song P-F, Zhu Y-D, Ma H-Y, et al. Discovery of natural pentacyclic triterpenoids as potent and selective inhibitors against human carboxylesterase 1. *Fitoterapia*. 2019;137.

38 Yao M, Ma X, Zhang X, et al. Lectin-mediated pH-sensitive doxorubicin prodrug for pre-targeted chemotherapy of colorectal cancer with enhanced efficacy and reduced side effects. *Theranostics*. 2019;9:747–760.

39 Rivory LP, Riou JF, Haaz MC, et al. Identification and properties of a major plasma metabolite of irinotecan (CPT-11) isolated from the plasma of patients. *Cancer Res*. 1996;56:3689–3694.

40 Rafiq M, Saleem M, Hanif M, Kang SK, Seo SY, Lee KH. Synthesis, structural elucidation and bioevaluation of 4-amino-1,2,4-triazole-3-thione's Schiff base derivatives. *Arch Pharm Res*. 2016;39:161–171.

41 Chae J, Choi I, Kim C. Homology modeling and molecular docking study of translationally controlled tumor protein and artemisinin. *Arch Pharm Res*. 2006;29:50–58.

42 Kong TY, Kim JH, Kim DK, Lee HS. Synthetic cannabinoids are substrates and inhibitors of multiple drug-metabolizing enzymes. *Arch Pharm Res*. 2018;41:691–710.